

Time Variability of the Geocoronal Solar Wind Charge Exchange in the Direction of the Celestial Equator

Yuichiro EZOE¹, Ken EBISAWA², Noriko Y. YAMASAKI², Kazuhisa MITSUDA², Hiroshi YOSHITAKE², Naoki TERADA³, Yoshizumi MIYOSHI⁴, and Ryuichi FUJIMOTO⁵

¹ *Tokyo Metropolitan University, 1-1, Minami-Osawa, Hachioji, Tokyo, 192-0397, JAPAN*

² *The Institute of Space and Astronautical Science (ISAS), Japan Aerospace and eXploration Agency (JAXA), 3-1-1 Yoshinodai, Sagamihara, Kanagawa 229-8510, JAPAN*

³ *Tohoku University, 6-3, Aoba, Aramaki-za, Sendai, Miyagi 980-8578, JAPAN*

⁴ *Nagoya University, Furo-cho, Chikusa-ku, Nagoya 464-8601, JAPAN*

⁵ *Kanazawa University, Kakuma-chou, Kanazawa, Ishikawa 920-1192, JAPAN*

ezoe@phys.metro-u.ac.jp

(Received ; accepted)

Abstract

We report the detection of a time variable OVII line emission in a deep 100 ks Suzaku X-ray Imaging Spectrometer spectrum of the Galactic Ridge X-ray emission. The observed line intensity is too strong (11 ± 2 line unit or photon $\text{cm}^{-2} \text{s}^{-1} \text{str}^{-1}$) to be emitted inside the heavily obscured Galactic disk. It showed a factor of two time variation which shows a significant ($\sim 4\sigma$) correlation with the solar wind O^{7+} ion flux. The high line intensity and the good time correlation with the solar wind strongly suggests that it originated from geocoronal solar wind charge exchange emission. We discuss the X-ray line intensity considering a line of sight direction and also theoretical distribution models of the neutral hydrogen and solar wind around the Earth. Our results indicate that X-ray observations of geocoronal solar wind charge exchange emission can be used to constrain these models.

Key words: X-ray: diffuse background — Sun: solar wind — Sun: solar-terrestrial relations — Earth

1. Introduction

The solar wind charge exchange (SWCX) emission has been recognized to reproduce X-ray emission in many solar system environments such as comets, geocorona, heliosphere, and planetary atmospheres (see Bhardwaj et al. 2007 for review). When an ion in the solar wind interacts with a neutral atom, it strips an electron(s) from the atom and X-ray or ultra-violet photon(s) are released as the electron relaxes into the ground state. Therefore, the SWCX

spectrum is characterized by strong emission lines from highly ionized atoms such as O^{7+} or C^{5+} . It can be distinguished from ordinary thermally equilibrium plasma emission by strong emission lines from large principle quantum number states such as $n=3-6$, and strong forbidden lines. The classical over-the barrier model (Ryufuku et al. 1980; Mann et al. 1981) can explain the large n line feature. Because the heavy solar wind ions are highly charged, their ionization potentials are larger than those of the neutral target. Therefore, when the electron moves from the target to the ion, it transfers into an excited state of the ion whose potential most closely matches that of the neutral. Consequently, the electron will enter into a high n state and then emit a strong emission line by the transition. The strong forbidden line feature is explained by a statistical-distribution model (Krasnopolsky et al. 2004).

Among many classes of SWCX objects in the solar system, the geocorona is now considered as an important contamination. The low density neutral hydrogen around the Earth or the geocorona emits X-ray emission lines such as O VII, O VIII, and C V K_α by the SWCX. When we would like to observe soft X-rays from objects such as clusters of galaxies, this component can be a contamination source. At the same time, SWCX X-ray emission can provide a diagnostic of the spatial distribution of the geocorona and solar wind near the Earth.

During the ROSAT all-sky survey, Snowden et al. (1994) found unknown long term enhancements (LTE) in the soft X-ray background. Motivated by the discovery of cometary X-rays (Lisse et al. 1996; Dennerl et al. 1997), Cox (1998) suggested that the SWCX due to geocorona can explain a part of the LTE. Robertson & Cravens (2003) constructed a model to simulate a spatial distribution of the geocoronal SWCX emission using the Earth's exosphere and solar wind distributions.

Observational results, which supports these predictions, have been taken with Chandra, XMM-Newton, and Suzaku. Wargelin et al. (2004) found a signature of an oxygen emission line in the Chandra Moon observation. Because the Moon occults any background sources, it must have originated from the geocoronal SWCX. Snowden et al. (2004) discovered a significant enhancement of the soft X-ray background during one of XMM-Newton's observations of the Hubble Deep Field-North. The emission showed lines from O, Ne and Mg and also was time variable. This phenomena was nicely explained by XMM-Newton's changing viewing geometry with respect to the geocorona, whose SWCX is predicted to have a specific distribution around the Earth (Robertson & Cravens 2003).

Carter & Sembay (2008) systematically investigated XMM-Newton archival data focusing on time variability of the soft X-ray background. Using solar wind data and considering the XMM-Newton's line of sight, similar to Snowden et al. (2004), they found that, in several cases, the SWCX enhancement occurred when XMM-Newton was on the sub-solar side of the magnetosheath which is predicted by Robertson & Cravens (2003) to be a high SWCX flux region. The SWCX-like emission was found for other cases when XMM-Newton had a line of sight which did not intersect the high flux region. They considered that these probably

arise from a non geocoronal origin such as a coronal mass ejection (CME) passing through the heliosphere.

CMEs have been used to explain diffuse X-ray background in other X-ray observations. For example, Carter & Sembay (2010) recently reported a diffuse variable X-ray emission detected with XMM-Newton. They analyzed its spectrum and light curve in combination with the solar wind proton data, and concluded that this is associated with a CME which interacted with neutrals in the Earth's exosphere.

Thanks to a good energy response of the CCDs onboard Suzaku, Fujimoto et al. (2007) discovered a firm line of evidence for the geocoronal SWCX emission in the north ecliptic pole observation (RA= 272.800°, Dec= 66.000°, J2000). Although the observation was originally conducted to take the sky X-ray background, they found a variability in X-ray CCD light curves, which apparently correlates with the solar wind proton flux. They divided the data into two periods, i.e., the stable and flare durations and successfully found enhancement of emission lines such as the C VI 4p to 1s line and the O VII forbidden line, in the flare spectrum. To explain short-term variations of less than 1 hr, they introduced a new parameter, the point where the line of sight encounters the magnetosheath (see figure 8 in Fujimoto et al. 2007). They concluded that the short-term X-ray variability have anti-correlation with the distance to the magnetosheath.

In this paper, we studied a possible SWCX oxygen line emission discovered in the long Suzaku observation of the Galactic ridge (RA= 281.000°, Dec= -4.070°, J2000), ($l = 28.46^\circ$, $b = -0.20^\circ$). In Ebisawa et al. (2008), we found strong O VII emission which is difficult to attribute to the Galactic ridge X-ray emission. Although we thought that it can be the SWCX emission, investigations are not enough to conclude that. In this paper, to confirm this inspection, we conducted a timing analysis by combining the Suzaku data with the solar wind data. While the north ecliptic pole observation was in the direction of the north pole, the Galactic ridge is near the celestial equator and the sub-solar side of the magnetosheath, where the geocoronal SWCX is expected to be strong. The good statistics 100 ks Suzaku data provides us with a good opportunity to characterize the geocoronal SWCX emission.

2. Observation

The Suzaku observation of the Galactic Ridge direction was conducted from 2005 October 28, 02:24 to October 30, 21:30 for 100 ks. October 28 and 30 corresponds to the Day of Year (DOY) in 2005 of 301 and 303, respectively. Suzaku (Mitsuda et al. 2007) is the fifth Japanese X-ray astronomical satellite which carries four X-ray CCDs (X-ray Imaging Spectrometer, XIS; Koyama et al. 2007). Due to the low-earth orbit and the large effective area, the back-illuminated type CCD (XIS1) has one of the lowest relative particle backgrounds among all X-ray CCDs in currently available X-ray observatories. Furthermore, the XIS1 has good energy resolution and superior low-energy response with negligible low-energy tails. These

two characteristics make Suzaku ideal for studying diffuse soft X-ray emission like the geocoronal SWCX.

Figure 1 shows the XIS spectra in the low energy band taken from Ebisawa et al. (2008). Among many emission lines such as Fe XVII (0.829 ± 0.004 keV), Ne X (1.021 ± 0.002 keV), Mg XI (1.342 ± 0.003 keV), and Si XIII (1.843 ± 0.003 keV), we can notice a strong O VII line at 0.560 ± 0.03 keV. These energies are the best fit values in table 2 of Ebisawa et al. (2008). The line center energy of O VII is more likely the forbidden line (561 eV) than the resonance line (574 eV). Its intensity is too strong to arise from the Galactic ridge X-ray emission which must suffer from the interstellar hydrogen column density of $N_H \sim 1 \times 10^{21}$ cm². The flux is $(320 \pm 50) \times 10^{-5}$ photons s⁻¹ cm⁻² deg⁻², which corresponds to 11 ± 2 line units (LU, photons s⁻¹ cm⁻² str⁻¹). This is even larger than that of the O VII line due to SWCX found in the north ecliptic pole observation ($5.1^{+1.1}_{-1.0}$ LU, Fujimoto et al. 2007),

This strong O VII emission line motivated us to investigate the light curve in detail. Below we use only the back-illuminated CCD (XIS1) data since it has the higher statistics for the oxygen line compared to the front-illuminated CCDs as shown in figure 1. The data reduction was performed in the same way as Ebisawa et al. (2008) except that the HEASoft analysis package was ver 6.1.1.

3. Timing Analysis

To examine the SWCX interpretation, we created the XIS1 light curve in 0.5–0.65 keV where the O VII line dominates and compared it with solar wind data. Similar to Ebisawa et al. (2008), we excluded two point sources within the field of view (Suzaku J1844–0404 and G28.6–1), in order to avoid contamination from these sources. The total area after removing two regions is 275 arcmin². Figure 2 shows the XIS1 0.5–0.65 keV light curve in 8192 s bins, compared to the WIND proton and ACE O⁷⁺ ion fluxes¹. The position of WIND during the observation was +200 R_E (Earth radius) and –50 R_E in the GSE x-y coordinates (i.e., at the pre-bowshock position²), while ACE orbited around the Lagrangian point L₁ between the Sun and the Earth. Because the ACE level 2 (publication-quality) proton data was unavailable during a part of the observation, we used the WIND data for the proton flux. The average XIS1 count rate was 1.5×10^{-2} cts s⁻¹.

We can see an increase of the XIS1 light curve from 303 to 304 day. We checked the XIS1 light curves in different energy bands (0.65–1 keV and 1–10 keV) but both of them did not show such a variability (see fig. 2). Hence, this feature seems to be intrinsic for the O VII line emission. A similar enhancement can be seen in the solar wind proton and O⁷⁺ fluxes. Since the O⁷⁺ ion is the source for the SWCX O VII line which is from O⁶⁺, this provides a strong

¹ The WIND and ACE data were taken from ftp://space.mit.edu/pub/plasma/wind/kp_files/ and <http://www.srl.caltech.edu/ACE/ASC/level2/index.html>, respectively.

² http://cdaweb.gsfc.nasa.gov/cgi-bin/gif_walk

line of evidence that the O VII emission is truly arising from the SWCX. The heliospheric origin can be rejected since the heliosphere is far larger than the Earth’s geocorona in size and the short time variability of the solar wind will be smeared. Therefore, we conclude that the O VII line is likely from the geocoronal SWCX.

Because the ACE satellite orbits at the Lagrangian point L_1 and Suzaku is in the low Earth orbit, we can expect ~ 1 hr time delay between the XIS1 and ACE data. In order to examine the time delay, we conducted a cross-correlation analysis. This procedure needs that both light curves are taken in the equally-spaced time intervals. Since the time bins of ACE O⁷⁺ flux and XIS1 light curve are different, we interpolated the ACE data to match the XIS1. Considering the ACE O⁷⁺ flux is a 2 hr average, both the XIS and ACE data were binned into 8192 s. We then utilized `crosscor` in the HEASoft analysis package, to obtain the cross correlation. In this software, we can choose several parameters for the calculation of the cross correlation function. We chose the default mathematical algorithm (**fast=1**, fast Fourier transform) and normalization method (**normalization=1**, no renormalization).

The calculated cross correlation is shown in figure 3. At the time delay around 0~16384 s, the correlation coefficient was ~ 0.72 with the null hypothesis probability of 1×10^{-4} corresponding to $\sim 4\sigma$ significance. Hence, the correlations around the time delay of 0~16384 s are highly significant. We noticed that the peak is slightly shifted to the positive delay side, which means that the ACE data has a time delay against the XIS. This coincides with the fact that the ACE satellite orbits at the L_1 point and hence detects the solar wind before Suzaku. The expected time delay roughly depends on the distance between the two satellite ($\sim 1.5 \times 10^6$ km) and the average solar wind proton speed at the observation time (~ 400 km s⁻¹). Then, the time delay is estimated as ~ 3800 s. This is consistent with the observed time delay of 0~16384 s. The sparse ACE flux data hindered us to investigate a more accurate determination. Below we simply assume the time delay of 8192 s, corresponding to the peak of the cross correlation.

In figure 4, we plot a relation between the XIS O VII line rate and the ACE O⁷⁺ flux considering the time delay of 8192 s. We fitted the data with a linear function (solid line). The best-fit function was expressed as,

$$C_{\text{XIS1}} [\text{cts s}^{-1}] = C_{\text{O}^{7+}} [10^5 \text{ cm}^{-2} \text{ s}^{-1}] \times (7.8 \pm 1.3) \times 10^{-2} + (1.0 \pm 0.1) \times 10^{-2}, \quad (1)$$

where C_{XIS1} and $C_{\text{O}^{7+}}$ are the XIS1 0.5–0.65 keV count rate and the ACE O⁷⁺ flux, respectively. The error is 1σ statistical one. The reduced χ^2 was 0.32 for 25 degree of freedom and hence acceptable. This relation suggests that a linear increase of the XIS1 count rate according to the ACE O⁷⁺ flux, which coincides with the SWCX picture. To know the effect of the assumed time delay on the relation, we tested other values (0 and 16384 s). We found that, even in these cases, the best-fit linear and constant coefficients coincide with those assuming 8192 s within 1σ fitting errors.

We noticed that, even if the solar wind O⁷⁺ flux is zero, there remains a certain offset

component. This is considered to consist of the instrumental and sky background. To clarify the offset component, we estimated the instrumental background using the XIS background data base, which was built from night Earth observations (Tawa et al. 2008), in the same way as Ebisawa et al. (2008). The XIS1 0.5–0.65 keV instrumental background was estimated as $(3.9 \pm 0.1) \times 10^{-3}$ cts s⁻¹ which occupies 40 % of the offset value. The rest must be a stable background from the sky, $(0.6 \pm 0.1) \times 10^{-2}$ cts s⁻¹ corresponding to ~ 4 LU in flux.

The most plausible interpretation for this sky background is a sum of the heliospheric SWCX and the soft X-ray background. The former occurs when the solar wind ions react with a neutral target in the heliosphere (e.g., Koutroumpa et al. 2007) but its contribution is unclear, since it is observationally difficult to distinguish the heliospheric SWCX from the geocoronal SWCX except by time variations. The latter is considered to consist of faint extragalactic sources and emission from highly ionized ions in solar neighborhoods and in our Galaxy (e.g., McCammon et al. 2002; Masui et al. 2009; Yoshino et al. 2009). Recently, Masui et al. (2009) studied the soft X-ray background from the galactic disk ($l = 235^\circ$, $b = 0^\circ$) with Suzaku. The O VII line flux in this line of sight was 2.93 ± 0.45 LU. The line of sight of our Galactic ridge observation ($l = 28.463^\circ$, $b = -0.204^\circ$) is in the direction of the galactic disk. The slightly different flux may be due to possible directional dependence of the soft X-ray background and/or seasonal or directional differences in the heliospheric SWCX.

As an additional background, we also considered the fluorescence scattering of solar X-rays by the Earth’s atmosphere. The fluorescent oxygen line at 0.53 keV is sometimes seen in past Suzaku observations (e.g., Miller et al. 2008). The contribution of the fluorescent emission line depends on both the amount of the solar X-rays during the observation and the Earth’s atmosphere density along the line of sight, which is related to the telescope elevation angle from the Earth (ELV). To estimate this influence, we filtered the XIS1 data with different ELV of $> 5^\circ$ (default criteria), $> 10^\circ$, $> 20^\circ$, $> 30^\circ$, and $> 50^\circ$. We then found no significant change in the count rate when the ELV criteria is different. This suggests a negligible contribution from the fluorescence scattering. This is consistent with the fact that the solar X-rays were quite stable at a low level during the observation ($7 \times 10^{-7} \sim 3 \times 10^{-8}$ W m⁻² in the GOES12 1.0–8.0 Å data)³. This flux level corresponds to the minimum class solar flare (class A) or less. Hence, we concluded that the fluorescent scattering of solar X-rays is negligible in our data.

4. Discussion

We analyzed the Suzaku XIS1 Galactic ridge observation data and discovered a good time correlation between the XIS1 O VII count rate and the ACE O⁷⁺ ion flux. From the line center energy and the time correlation with the solar wind, we concluded that this emission originates from the geocoronal SWCX. The average O VII line flux was 11 LU, composed of 7

³ <http://www.swpc.noaa.gov/>

LU from the geocoronal SWCX and 4 LU from the sky background including the soft X-ray background and the heliospheric SWCX. Below, we discuss the expected line intensity of the geocoronal SWCX.

Figure 5 shows the schematic view of the Earth’s magnetosphere and line of sight in our observation. While the north ecliptic pole observation with Suzaku was in the direction of the north pole (Dec= 66°) (Fujimoto et al. 2007), the line of sight in this observation is almost vertical to it (Dec= -4°). The line of sight corresponds to the sub-solar side of the magnetosheath which is predicted to be a high SWCX flux region by the theoretical model (Robertson & Cravens 2003).

The line of sight of the Galactic ridge also makes a clear difference in the geocentric distance of the point whose geomagnetic field becomes open to space for the first time along the line of sight (r_{mp} , see fig. 5 for definition). This definition is the same as that in Fujimoto et al. (2007). In our case, it is equal to the line-of-sight distance to the magnetopause boundary which is the location where the outward magnetic pressure balances the solar wind pressure. Here r_{mp} is an important parameter to estimate the geocoronal SWCX intensity because most of the solar wind are blocked by the Earth’s magnetic field and hence interact around r_{mp} . Since the Earth’s exospheric density strongly depends on the distance from the Earth (e.g., Ostgaard et al. 2003), r_{mp} should have a large impact on the SWCX intensity.

Fujimoto et al. (2007) evaluated r_{mp} using the software GEOPACK-2005 and T96 magnetic field model (Tsyganenko et al. 2005)⁴. In this model, they took into account solar wind parameters, that can influence on the structure of the magnetosphere, using CDAWeb (Coordinated Data Analysis Web)⁵. We calculated r_{mp} in the same way and found that it is almost constant around $\sim 12 R_E$, corresponding to the distance to the magnetopause. This is natural consequence if we consider the line of sight direction (see fig. 5). r_{mp} is larger than that in the north ecliptic pole ($2\sim 8 R_E$). In order to investigate whether the short term variability seen in the north ecliptic pole was due to the changing r_{mp} , we checked the short term variability less than several hours by changing the bin size of the O VII light curve from 512 s to 8096 s in our data. Then we found no sign of such a variability, which is consistent with the almost constant r_{mp} .

We then proceeded to estimate the expected X-ray line intensity from an equation below,

$$f_{\text{OVII}} \sim \frac{1}{4\pi} \int_{l_{\text{min}}}^{l_{\text{max}}} \alpha f_{\text{O}^{7+}} n_{\text{H}}(l) dl \text{ [photon s}^{-1} \text{ cm}^{-2} \text{ str}^{-1}] \quad (2)$$

where f_{OVII} and $f_{\text{O}^{7+}}$ are the O VII line intensity and solar wind O^{7+} flux, n_{H} is the neutral geocoronal hydrogen density, and l is the line of sight. l_{max} and l_{min} are the most distant and closest distances at which the solar wind ions can interact with the neutral target. α contains the atomic cross section and transition probability information.

⁴ <http://modelweb.gsfc.nasa.gov/magnetos/data-based/modeling.html>

⁵ <http://cdaweb.gsfc.nasa.gov/cdaweb/sp phys/>

To calculate f_{OVII} , we made simple assumptions as below. We used α of $6 \times 10^{-15} \text{ cm}^{-2}$ from Wegmann et al. (1998), assuming that all transitions are equally probable. The Earth's exospheric neutral hydrogen density model by Ostgaard et al. (2003) was used for $n_{\text{H}}(l)$. Because most of the solar ions will be trapped near the Earth's magnetopause in the direction of the Galactic ridge, we simply assumed $l_{\text{min}} = r_{\text{mp}}$. l_{max} of $20 R_{\text{E}}$ was assumed as a rough estimate, because $n_{\text{H}}(l)$ at $>12 R_{\text{E}}$ is not well known due to the very low density ($< 20 \text{ cm}^{-3}$, see fig. 10 in Ostgaard et al. 2003). The average ACE O^{7+} ion flux of $\sim 1 \times 10^{-5} \text{ cm}^{-2} \text{ s}^{-1}$ was used as $f_{\text{O}^{7+}}$. Then, the O VII line flux was estimated as 0.2 LU, which was 35 times smaller than the observation. Even if we integrate the equation up to $100 R_{\text{E}}$, it was 0.3 LU, still 20 times smaller.

In the above calculation, we did not take into account an effect of the bow shock across which can increase the solar wind flux. Then, we tried to take into account this effect based on a standard theoretical model given by Spreiter et al. (1966). According to their calculation, the solar wind mass flux increases 2~3 times across the bow shock in the sub-solar side. Although we take into account this effect, there remains a factor of ~ 10 discrepancy between the observed and expected O VII line flux. This uncertainty can be due to an uncertainty of the neutral hydrogen model at $>10 R_{\text{E}}$ and/or the solar wind distribution.

The time delay between the X-ray light curve and the solar wind ion flux can provide us with information on the propagation of the solar wind. Carter & Sembay (2010) checked the ACE and WIND proton curves, and estimated the orientation of the solar wind wavefront assuming a planar wavefront. In our case, a part of the ACE proton flux during the time variation is unfortunately unavailable. On the other hand, as we described in §3, the time delay between the Suzaku light curve and the ACE ion flux of 0~16384 sec is consistent with the calculation assuming the planar wavefront and constant solar wind velocity. This supports that enhancement of the geocoronal SWCX diffuse X-ray background can be predicted and excluded if there are simultaneous solar wind proton and ion observations.

Finally, we point out that the geocoronal SWCX in combination with the solar wind data can be a useful tool to evaluate the Earth's exospheric density model and the solar wind distribution. Our observation had a line of sight which intersects with the sub-solar side of the magnetosheath, which is predicted to have a high SWCX flux. Archival Suzaku data analysis will enable us to examine the directional dependence even more. Our observation demonstrated that the time delay and intensity relationship between the X-ray O VII line and solar wind O^{7+} flux must be a key to investigate the line of sight dependence of the geocoronal SWCX. Future high-energy resolution observations with an X-ray microcalorimeter onboard Astro-H will make it possible to monitor the conditions of the Earth's exosphere and solar wind more precisely.

The authors acknowledge the Suzaku XIS instrument and operation team, and the ACE SWEPAM/SWICS instrument team and the ACE Science Center.

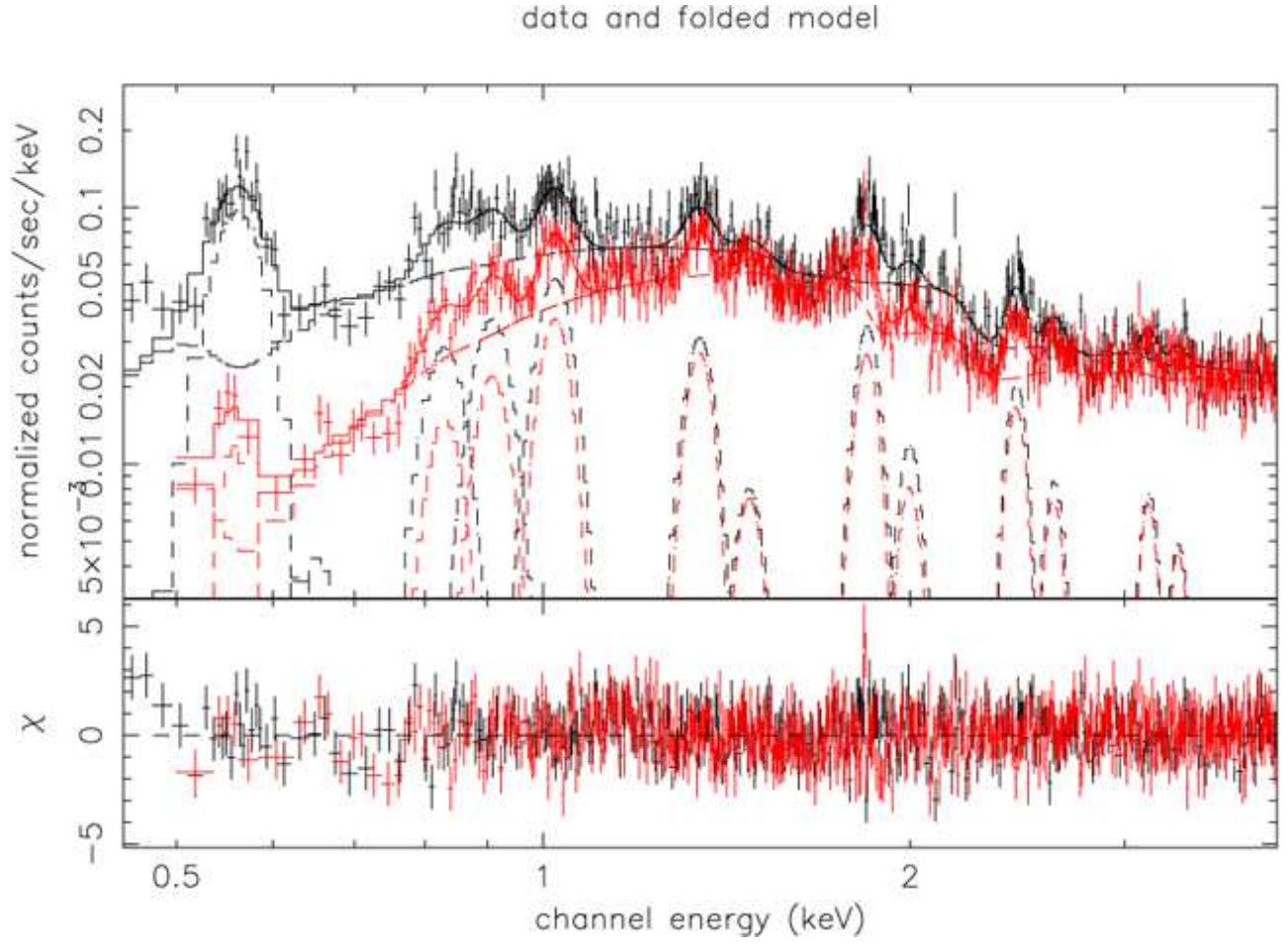


Fig. 1. Background-subtracted XIS1 (black) and XIS0 + 2 + 3 (red) spectra of the Galactic ridge region. The solid line is the best-fit power-law plus thirteen Gaussian model. The dashed lines are the model components. Parameters are described in table 2 of Ebisawa et al. (2008). The bottom panel indicates residuals of the data from the model.

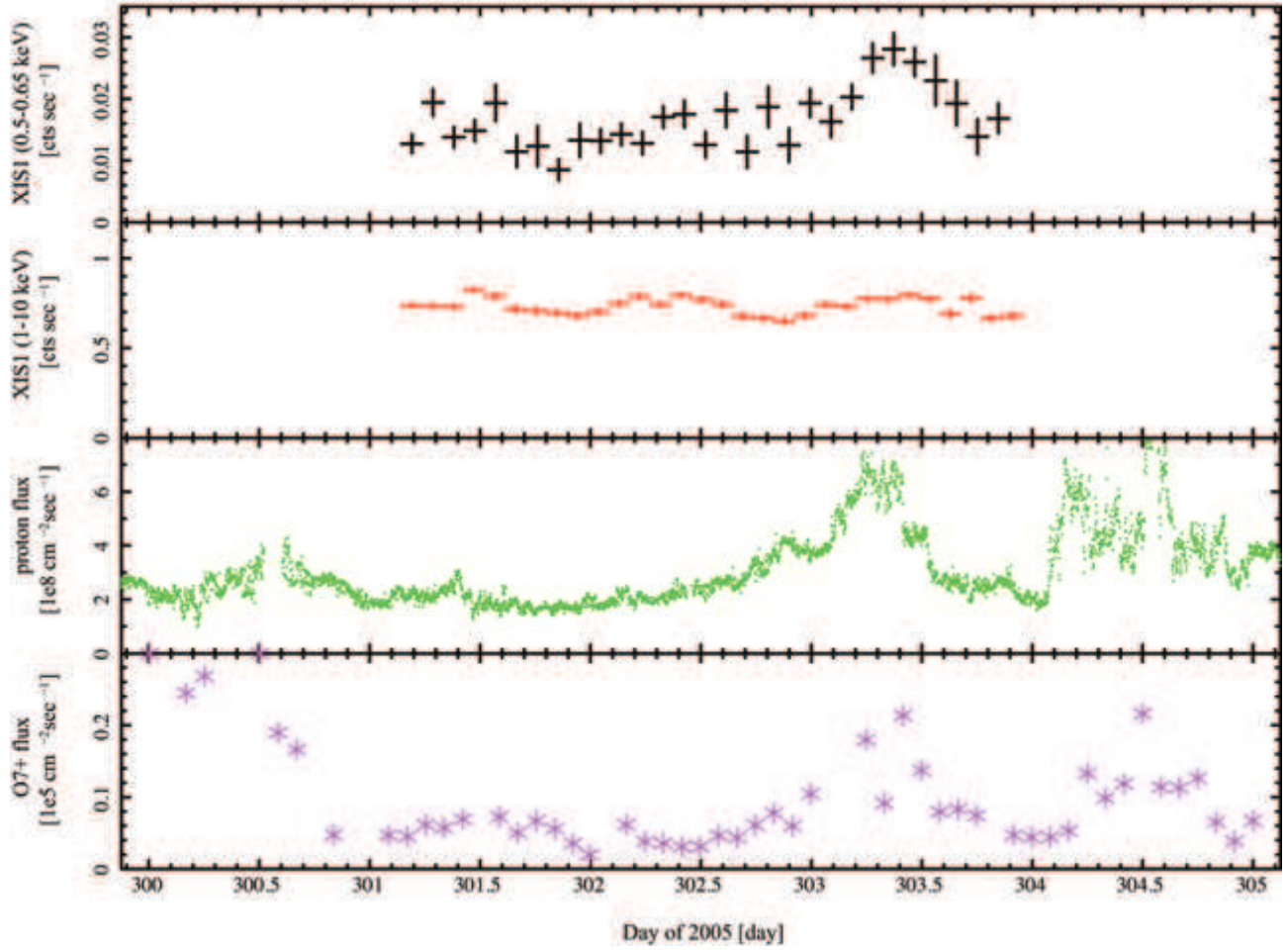


Fig. 2. XIS1 light curves in 0.5–0.65 keV and 1–10 keV, solar wind proton flux, and O⁷⁺ flux as a function of day of year (DOY) in 2005. The DOY of 301 corresponds to 2005 October 28. X-ray photons from calibration sources are excluded for the XIS1 1–10 keV light curve. The vertical error bars are at 1σ significance. The solar wind proton flux is calculated from WIND SWE data (0.001 day=86.4 sec average), while the O⁷⁺ flux is from level 2 ACE SWICS data (2 hr average, corresponding to the minimum time bin). Only good data with quality flag 0 were used for the ACE data.

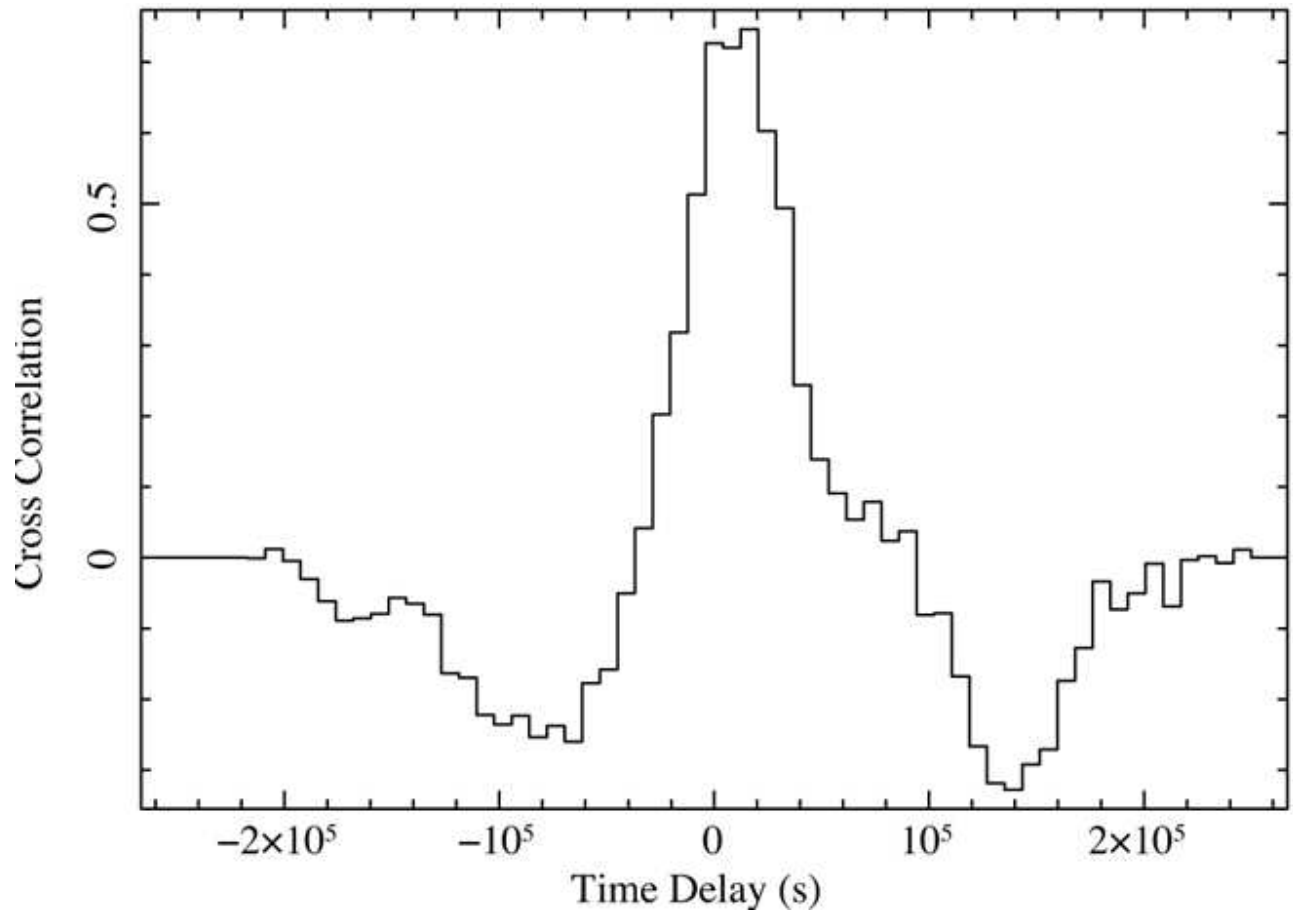


Fig. 3. Cross correlation between the XIS1 O VII line emission and ACE O⁷⁺ flux curves. A positive time delay means that the ACE data leads the XIS1.

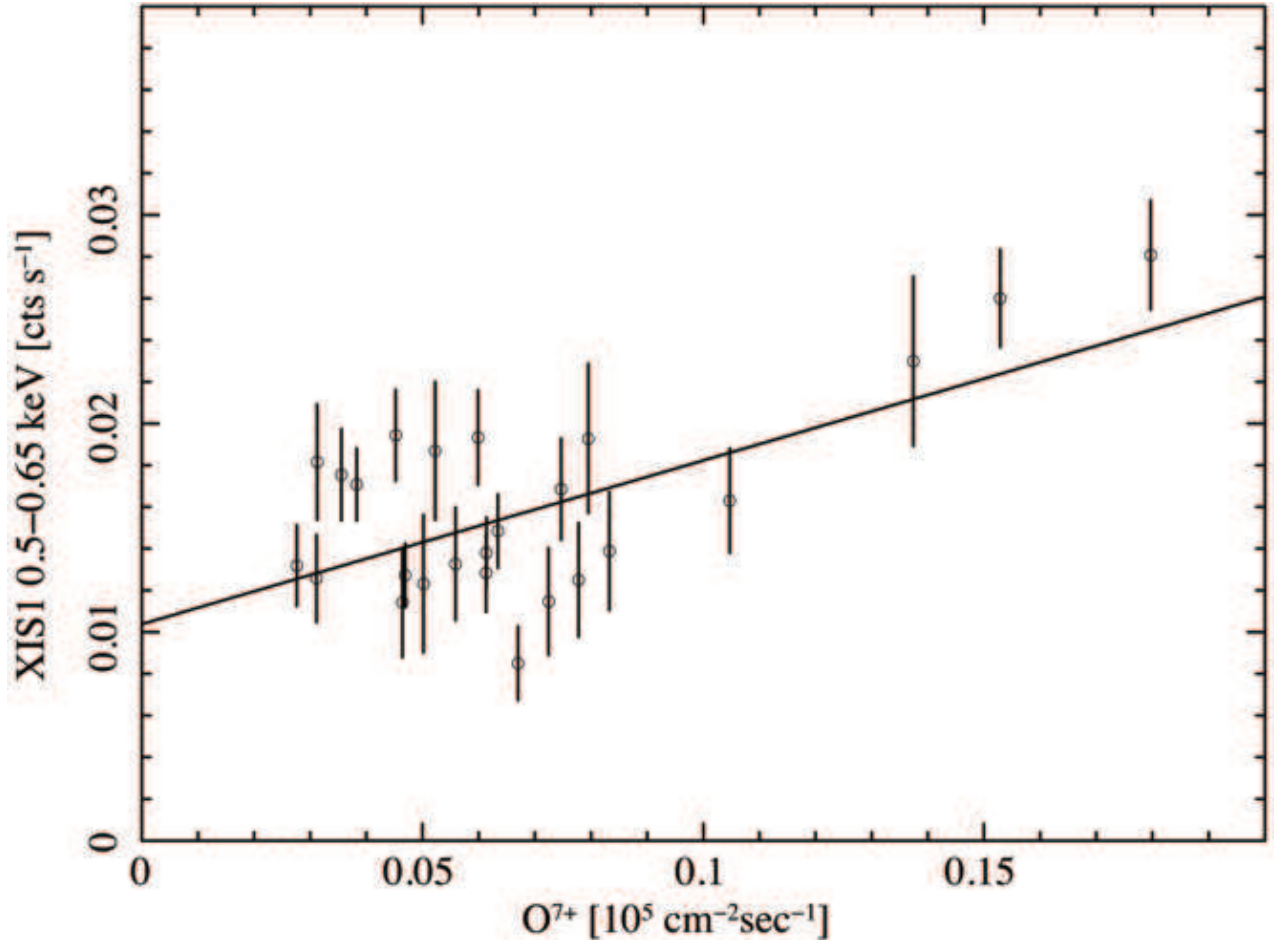


Fig. 4. Correlation between the XIS1 O VII line emission and ACE O⁷⁺ flux curves, considering the 8192 s time delay of the Suzaku data (see text in §3). The vertical error bar is at 1σ significance. The solid curve is the best-fit linear function.

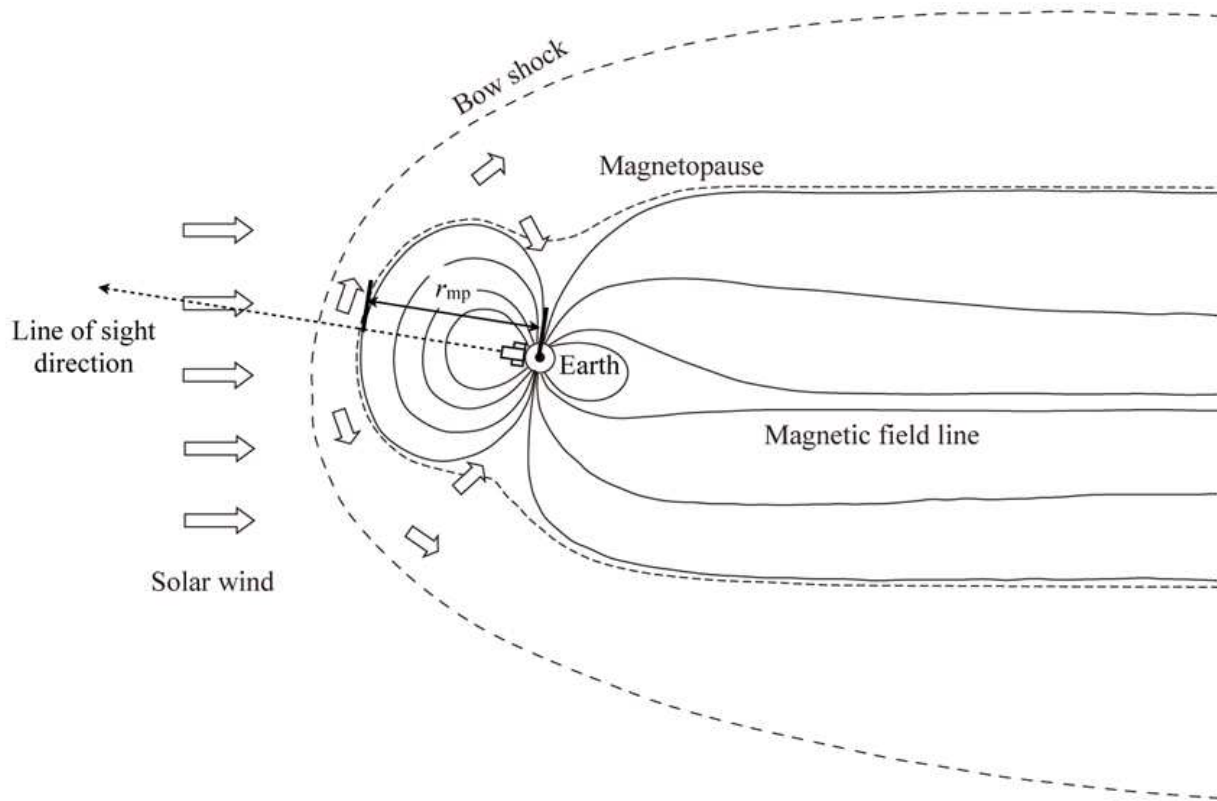


Fig. 5. Schematic view of the magnetosphere and line of sight of the satellite, observed in the GSE x-z plane. The Sun angle (Sun-Suzaku-object) during the observation was $\sim 67^\circ$ and the line of sight has a $+57^\circ$ azimuth angle, perpendicular to this diagram.

References

- Bhardwaj, A., et al. 2007, *Planetary & Space Sci.*, 55, 1135.
- Carter, J.A., & Sembay, S. 2008, *A&A*, 489, 837.
- Carter, J.A., Sembay, S., & Read, A.M. 2010, *MNRAS*, 402, 867.
- Cox, D.P. 1998, *The Local Bubble and Beyond*. (Springer, Berlin), 121.
- Dennerl, K., Englhauser, J., & Trumper, J. 1997, *Science*, 277, 1625.
- Ebisawa, K., et al. 2008, *PASJ*, 60, 223.
- Fujimoto, R., et al. 2007, *PASJ*, 59, S133.
- Koutroumpa D., Acero F., Lallement R., Ballet J., Kharchenko V., 2007, *A&A*, 475, 901.
- Koyama, K., et al. 2007, *PASJ*, 59, S23.
- Krasnopolsky, V. A., Greenwood, J. B., & Stancil, P. C. 2004, *Space Sci. Rev.*, 113, 271.
- Lisse, C.M., et al. 1996, *Science*, 274, 205.
- Mann, R., Folkmann, F., & Beyer, H. F., 1981, *J. Phys. B*, 14, 1161.
- Masui, K., et al. 2009, *PASJ*, 61, S115.
- McCammon, D., et al. 2002, *ApJ*, 576, 188.
- Miller, E. D., et al. 2008, *PASJ*, 60, 95.
- Mitsuda, K., et al. 2007, *PASJ*, 59, S1.
- Ostgaard, N., et al. 2003, *J. Geophys. Res.*, 108, A7.
- Robertson, I. P., & Cravens, T. E. 2003, *Geophys. Res. Lett.*, 30, 1439.
- Ryufuku, H., Sasaki, K., & Watanabe, T. 1980, *Phys. Rev. A.*, 21, 745.
- Snowden, S. L., McCammon, D., Burrows, D.N., Mendenhall, J.A. 1994, *ApJ*, 424, 714.
- Snowden, S. L., Collier, M. R., & Kuntz, K. D. 2004, *ApJ*, 610, 1182.
- Spreiter, J. R., Summers, A. L., & Alsne, A. Y. 1996, *Planet. Space. Sci.*, 14, 223.
- Smith, R. K., et al. 2007, *PASJ*, 59, 141.
- Tawa, N., et al. 2008, *PASJ*, 60, S11.
- Tsyganenko, N. A., & Sitnov, M. I. 2005, *J. Geophys. Res.*, 110, A03208.
- Yoshino, T., et al. 2009, *PASJ*, 61, 805.
- Wargelin, B. J., et al. 2004, *ApJ*, 607, 596.
- Wargelin, R., et al. 1998, *Planet. Space. Sci.*, 46, 603.